Experimental Mechanics (2020) 60:889–905
https://doi.org/10.1007/s11340-020-00596-3

RESEARCH PAPER

On the New Shear Constraint for Plane-Stress Orthotropic Plasticity Modeling of Sheet Metals

W. Tong[1] · **M. Alharbi**[2] · **J. Sheng**[1]

Received: 26 November 2018 / Accepted: 27 April 2020 / Published online: 15 June 2020

Abstract

Background A shear constraint was very recently proposed by Abedini et al. (Int. J. Solids and Structures **151**: 118–134 2018) to evaluate and calibrate advanced non-quadratic anisotropic yield criteria and to eliminate what they called non-physical numerical artifacts in those criteria.

Objective This investigation points out that such a shear constraint is in fact unnecessary for plane-stress orthotropic plasticity in general.

Methods Using the well-known Hill's 1948 quadratic and Gotoh's 1977 quartic yield functions for orthotropic sheet metals in plane stress, it is shown analytically that pure shear stressing and pure shear straining loading conditions are not equivalent except for very special cases. By conducting a series of shearing experiments on an aluminum sheet metal, the actual test results are shown not to provide any unequivocal supporting evidence at all to the newly proposed shear constraint.

Results The so-called non-physical numerical artifacts of the non-equivalence in pure shear stressing and pure shear straining of a sheet metal are in fact the intrinsic features of an anisotropic material in general.

Conclusions The newly proposed shear constraint should thus not be accepted to be universally applicable at all for anisotropic plasticity modeling of sheet metals. Such a proposed constraint itself shall be regarded as a provisional simplifying assumption of reduced anisotropy only for some particular sheet metals under consideration.

Keywords Anisotropic plasticity · Non-quadratic yield criterion · Orthotropic flow potential · Simple shear · Pure shear

Abbreviations

x,y,z The orthotropic material symmetry axes corresponding to the rolling (RD), transverse (TD), and normal (ND) directions of a thin sheet metal.

$\sigma_x, \sigma_y, \tau_{xy}$ Three in-plane Cartesian (two normal and one shear) components of an applied Cauchy stress $\boldsymbol{\sigma}$ in the orthotropic coordinate system of the sheet metal.

$\Phi_{2y}, Y_1, Y_2, Y_3, Y_4$ Hill's 1948 quadratic anisotropic yield stress function in plane stress and its three on-axis (Y_1, Y_2, Y_3) and one off-axis (Y_4) polynomial coefficients or material constants.

$\Phi_{2p}, P_1, P_2, P_3, P_4$ Hill's 1948 quadratic anisotropic plastic flow potential in plane stress and its three on-axis (P_1, P_2, P_3) and one off-axis (P_4) polynomial coefficients or material constants.

$\Phi_4, A_1, ..., A_9$ Gotoh's 1977 fourth-order anisotropic yield stress function in Cartesian stress components ($\sigma_x, \sigma_y, \tau_{xy}$) and its five on-axis ($A_1, ..., A_5$) and four off-axis ($A_6, ..., A_9$) polynomial coefficients or material constants.

$\sigma_1, \sigma_2, \theta$ The applied Cauchy stress $\boldsymbol{\sigma}$ represented in terms of so-called intrinsic variables according to R. Hill, namely, the in-plane principal stresses and the stress loading orientation angle between the major principal stress σ_1 and the rolling direction (RD) of the sheet metal.

$\dot{\varepsilon}_1, \dot{\varepsilon}_2, \theta'$ The in-plane principal plastic strain increments and the straining loading orientation angle between

✉ W. Tong
wtong@lyle.smu.edu

[1] Department of Mechanical Engineering, Lyle School of Engineering, Southern Methodist University, Dallas, Texas 75275-0337 USA

[2] Present address: Mechanical Engineering Department, College of Engineering-Unizah, Qassim University, Buraydah, Saudi Arabia

	the major principal plastic strain increment $\dot{\varepsilon}_1$ and the rolling direction (RD) of the sheet metal.
τ and $\dot{\gamma}$	The yield stress in stress-controlled pure shear loading and plastic strain increment in strain/displacement-controlled pure or simple shear loading.

Introduction

A macroscopic anisotropic plasticity model that can adequately capture the directional and multi-axial dependence of the yielding, plastic flow, and strain hardening behavior of a sheet metal is often required in analyzing and simulating an industrial forming operation of the sheet metal. The phenomenological approach treats the sheet metal as a continuum and often formulates a general mathematical framework of macroscopic anisotropic plasticity in terms of a stress-based yield function [15, 23, 24]. At present, a yield function that is calibrated via experimental inputs from mechanical tests is still most widely used in industrial sheet metal applications as it is both more accurate and computationally more efficient [5].

In principle, any scalar-valued function of the Cartesian stress components of the plane stress tensor $\boldsymbol{\sigma} = (\sigma_x, \sigma_y, \tau_{xy})$ can be used as the plane stress yield function $f(\sigma_x, \sigma_y, \tau_{xy})$ for a sheet metal as long as it is both physically consistent and mathematically concise and well-posed. In practice, three types of constraints are imposed on a yield function of a sheet metal in terms of their degrees of generality. The most fundamental and basic constraint is to require a yield function to be positive and convex [9, 16, 18, 23, 24, 34]. The second level of constraints are often imposed in metal plasticity, including pressure-insensitive yielding, plastic incompressibility [14, 15], and an associated (or occasionally a non-associated) flow rule [9, 18]. The third level of constraints may often be regarded as *simplifying* constitutive assumptions of a reduced degree of anisotropy about strain hardening and material symmetry of a particular metal under consideration due to lack of relevant experimental inputs. Depending on the need to balance the model complexity and capabilities, various strain hardening features (isotropic, kinematic, differential, and anisotropic) and various degrees of material anisotropy (isotropic, planarly isotropic, orthotropic, and monoclinic) have been considered for sheet metal modeling in the past. A constitutive assumption about the so-called central asymmetry (that is, tension-compression asymmetry or strength differential effect) also belongs to the third type of provisional constitutive modeling constraints in metal plasticity.

Abedini et al. [2] recently proposed a new shear constraint in their evaluation and calibration of the non-quadratic anisotropic yield stress function YLD2000-2D for two aluminum sheet metals AA2090-T3 and AA7075-T6 in plane stress. Specifically, they insist in Section Mechanics of Shear Deformation of their paper that the principal stress ratio σ_2/σ_1 and the principal plastic strain increment ratio $\dot{\varepsilon}_2^p/\dot{\varepsilon}_1^p$ should *in general* be the same as -1 for *any* orthotropic sheet metal under either pure shear stressing or pure shear straining loading conditions regardless of the loading orientation and the actual degree of plastic anisotropy in the sheet metal. In this study, we clarified first in Section Two Types of Pure Shear Loading Conditions on a Sheet Metal the difference between these two types of pure shear loading conditions often used in shear testing of a sheet metal and then the difference between the on-axis/off-axis and coaxial/non-coaxial loading conditions on an orthotropic material. We next showed in Section Modeling Pure Shear by Hill's Quadratic and Gotoh's Quartic Anisotropic Plastic Models the general equivalency of these two types of 45° off-axis pure shear loading conditions but the general non-equivalence of these two types of *on-axis* pure shear loading conditions as given by the well-established Hill's 1948 quadratic and Gotoh's 1977 quartic anisotropic yield functions[11, 14]. In Section Shearing Experiments and Results on an AA6111-T4 Sheet, we described the shearing experiments on an AA6111-T4 sheet based on two shear test coupon geometries commonly used for sheet metals. We presented in Section Discussion and Conclusions some relevant experimental results of these shearing tests which in fact do not support the proposed shear constraint. We further pointed out that the very approximate nature of any shearing test of sheet metals in practice would not strictly and unequivocally lend itself as the physical basis at all for the universal shear constraint newly proposed by Abedini et al.[2]. In other words, such a constraint is in fact one of *provisional* third type constraints that overly restricts the well-established Hill's and Gotoh's orthotropic yield functions by reducing their total numbers of independent material constants by at least 1 and 2 respectively.

Two Types of Pure Shear Loading Conditions on a Sheet Metal

Shear testing and its three special cases

As the terms *shear*, *pure shear*, and *simple shear* are all used in the literature to the so-called shear testing [21, 26, 42], a concise definition will be given at first for rolled sheet metals. We adopt the principal stresses and the loading orientation angle $(\sigma_1, \sigma_2, \theta)$ or the intrinsic variables as called by Hill [19] to characterize the mechanical loading of a flat sheet metal element in plane stress[1].

[1]Per the 2D coordinate transformation of stress tensor, one has $\sigma_x = \sigma_1\cos^2\theta + \sigma_2\sin^2\theta$, $\sigma_y = \sigma_1\sin^2\theta + \sigma_2\cos^2\theta$, $\tau_{xy} = (\sigma_1 - \sigma_2)\sin\theta\cos\theta$.

So $\sigma_1 > \sigma_2 \geq 0$ defines biaxial tension (uniaxial tension when $\sigma_2 = 0$) while $\sigma_1 > 0$ and $\sigma_2 < 0$ is the stress state of a material element in an in-plane shear test. If the in-plane shear test is done under displacement boundary conditions, then the principal plastic strain increments and the straining orientation angle $(\dot{\varepsilon}_1^p, \dot{\varepsilon}_2^p, \theta')$ should be used instead. As it is usually understood for an orthotropic sheet, the mechanical loading is on-axis if $\theta = 0^o$ or $\theta = 90^o$ and it is off-axis when otherwise. Furthermore, the mechanical loading is coaxial in stress and strain if $\theta' = \theta$ and it is non-coaxial in stress and strain when $\theta' \neq \theta$. For orthotropic sheet metals, on-axis loading is always coaxial but off-axis loading may or may not be coaxial. For finite deformation including cases of only small strain but finite rotation, the in-plane material spin $\dot{\omega}$ should also be specified as part of either stress or strain controlled loading conditions on the sheet metal test piece.

The following three cases are most relevant to our discussion here: pure shear stressing, pure shear straining, and simple shear (straining). Pure shear stressing refers to pure shear in stress in most standard textbooks on mechanics of materials (see, e.g., page 33 of [13]) and in the anisotropic plasticity literature (see [6, 39]). As a plane-stress yield function in anisotropic plasticity is most often formulated using the applied Cauchy stress $\boldsymbol{\sigma}$, the ideal shear test condition would be under pure shear in stress, that is, $\sigma_1 = -\sigma_2 > 0$, see Fig. 1(a). This may be accomplished in principle using a biaxial test machine with no material spin [6, 38]. A free-end torsion test of the thin-walled tube may be approximated as a pure shear stress test with a finite material rotation if the hoop stress is zero [40].

In classical studies of elasticity and fracture mechanics of flat rubber samples, the pure shear strain test consisting of a thin rectangular rubber strip held by rigid clamps along its two long edges is often used [42]. Such a test should be more precisely called as the *out-of-plane* pure shear strain test or the in-plane plane strain stretching for a flat test piece without material rotation. The equivalence of pure shear straining and plane-strain stretching (on two different planes of the same test piece) is due to the material incompressibility in rubber elasticity. Similarly as shown in Fig. 1(b), *in-plane* pure shear plastic straining $\dot{\varepsilon}_1^p = -\dot{\varepsilon}_2^p > 0$ or $\dot{\varepsilon}_1^p + \dot{\varepsilon}_2^p = -\dot{\varepsilon}_3^p = 0$ would automatically require no thickness change in a sheet metal due to plastic incompressibility. It is thus equivalent to the *out-of-plane* plane strain stretching $(\dot{\varepsilon}_1^p > 0, \dot{\varepsilon}_3^p = 0)$.

In-plane shear tests reported in the literature for sheet metals [4, 8, 10, 21, 25, 30] are however more commonly referred to as simple shear (straining) in plane stress, see Fig. 1(c). Unlike in a fixed end torsion test of thin-walled tubes, those in-plane shear tests of a sheet metal in either double-shear [25] or single-shear [30] configurations do not fully and accurately prescribe the displacement boundary conditions on all four sides of a narrow rectangular gauge section as dictated by the simple shear deformation [3, 26, 27]. Instead, the narrow rectangular gauge section of a sheet metal test piece is sheared along its two long edges while its two short edges are actually stress free. Both the free edge effect and short (narrow) gauge length make the actual stress and strain states in the gauge section of such a test piece rather non-uniform and complex [3, 8, 29]. Even though the center gauge region of the sheet metal shear test piece may undergo the plastic deformation very close (but nevertheless not completely identical) to simple shear at finite strain levels [29], the overall quality and fidelity of the stress and strain measurement data in an in-plane simple shear test is thus rather inferior to those obtained from a standard uniaxial tensile test. Another significant difference between the simple shear and uniaxial tension tests is the large material rotation in finite simple shear. As the initial yielding is the focus in our current investigation, pure shear straining and simple shear straining may be treated equivalently in this context (i.e., the material rotation is small at the initial stage of plastic yielding in simple shear).

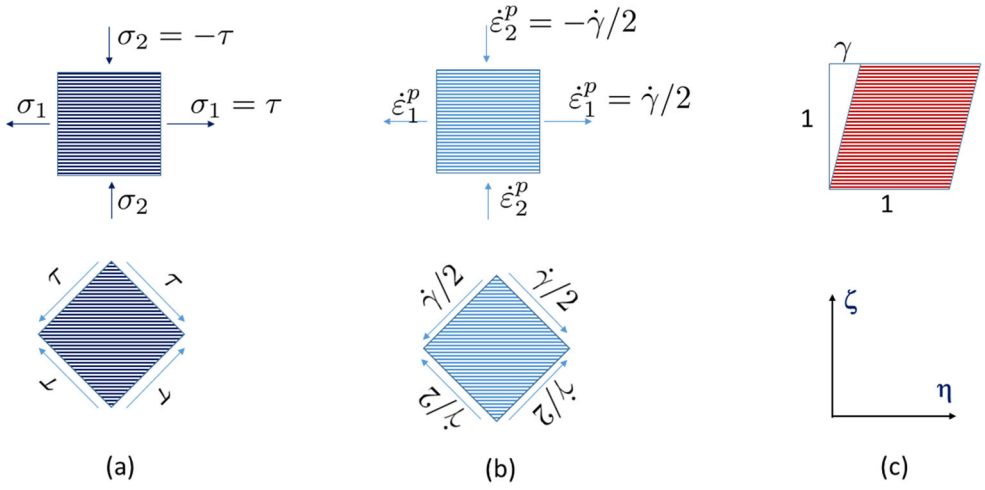

Fig. 1 **a** Pure shear stressing; **b** pure shear straining; **c** simple shear (straining) of a unit sheet metal element with the fixed laboratory coordinate axes $\eta\zeta$. Here the in-plane material symmetry axes xy with the horizontal rolling marks are aligned with the loading axes $\sigma_1\sigma_2$ and $\dot{\varepsilon}_1\dot{\varepsilon}_2$ as well as with the laboratory coordinate axes $\eta\zeta$. They are in general at a certain angle θ, θ' and ξ respectively

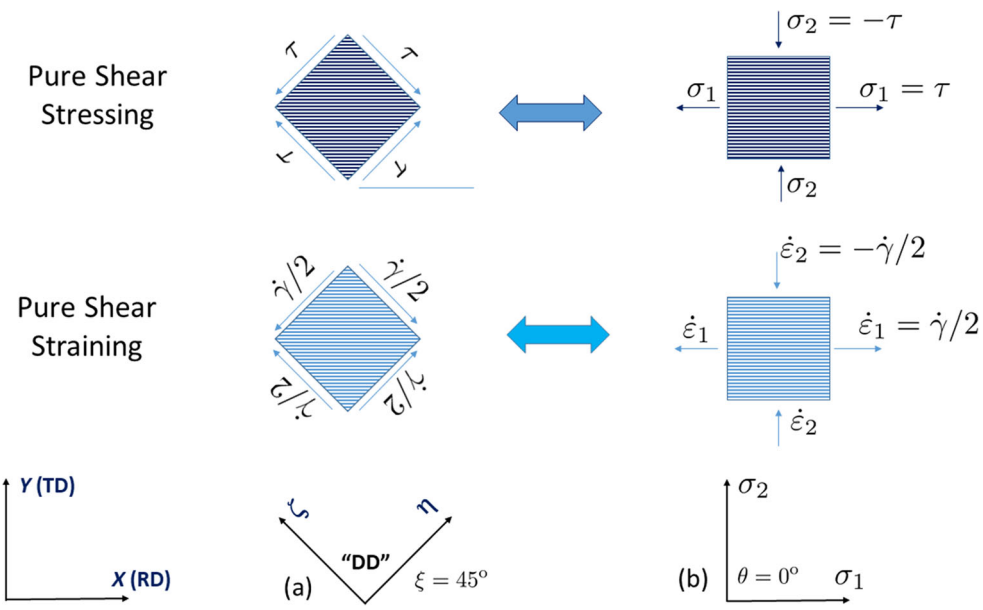

Fig. 2 Pure shear stressing and straining of a sheet metal at 45-degree diagonal direction to its material coordinates xy: **a** the DD material element edges aligned with the laboratory (shearing) coordinates $\eta\zeta$; **b** the material element edges aligned with principal stress axes $\sigma_1\sigma_2$

Selected on-axis and off-axis pure shear loading conditions

It is very important to clearly distinguish three coordinate systems commonly used in modeling and testing sheet metals in plane stress, namely, 1) the sheet metal material symmetry axes xy (corresponding to the rolling and transverse directions of a sheet metal), 2) the principal stress axes $\sigma_1\sigma_2$, and 3) the laboratory test coordinates $\eta\zeta$. We give first in this subsection a somewhat detailed description of four *coaxial* pure shear loading cases applied to a sheet metal in terms of these three coordinate systems, see Figs. 2, 3, 4 and 5. The first three pure shear cases considered here correspond to the stress state points ①, ② and ③ depicted in Fig. 3 of [2]. For simplicity, we treat the elastic deformation to be negligible in the following analysis[2] and exclude any rigid body motion. There are two types of the shearing loading conditions commonly applied to a unit square material element: pure shear stressing and simple shear straining. The term "stressing" is used here to emphasize the point that this particular pure shear is a stress-controlled loading condition. Similarly, the term "straining" is used along with simple shear to highlight that such a loading condition is strain-increment (displacement) controlled. To be specific, we define the laboratory test coordinates $\eta\zeta$ to be along the directions of the shearing stresses $\tau > 0$ or plastic shear strain increments $\dot{\gamma}/2 > 0$. One peculiar feature of 45° *off-axis* pure shear loading conditions is the coincidence of the principal stress axes $\sigma_1\sigma_2$ in stress-controlled loading and principal plastic strain increment axes $\dot{\varepsilon}_1\dot{\varepsilon}_2$ in strain-controlled loading (see Figs. 3 and 5). Following the usual practice [2], the shear test samples are also designated as RD, DD and TD in terms of the *shearing* loading direction and the rolling direction of a sheet metal. In an ideal pure shear stress test, the actual loading angle in terms of θ or θ' differs however from the RD, DD and TD uniaxial tensile test samples by 45°.

[2]So for simplicity, the superscript 'p' will be dropped in the rest of the manuscript for components of plastic strain increments

45-degree diagonal shearing $\xi = 45^o$ (on-axis loading $\theta = \theta' = 0^o$)

As shown in Fig. 2(a), either a pure shear stressing or straining condition is applied to a square unit material element aligned at a 45-degree angle from the rolling direction (x-axis) of the sheet metal (the DD shear test sample). The same stressing and straining conditions of 45-degree diagonal shearing may be described in terms of the unit material element aligned along the principal stress axes (and the sheet metal material symmetry axes too in this case) shown in Fig. 2(b). Using the Cartesian components in the sheet metal material symmetry coordinate system, the pure shear yield stress and plastic strain increment tensors shown in Fig. 2(a) are given respectively as

$$(\sigma_x, \sigma_y, \tau_{xy})_{ps1} = (\tau, -\tau, 0), \quad (\dot{\varepsilon}_x, \dot{\varepsilon}_y, \dot{\varepsilon}_{xy})_{ss1} = (\dot{\gamma}/2, -\dot{\gamma}/2, 0). \quad (1)$$

The same pure shear yield stress and plastic strain increment tensors in terms of the principal stress axes shown in Fig. 2(b) are given respectively as

$$(\sigma_1, \sigma_2, \theta)_{ps1} = (\tau, -\tau, 0), \quad (\dot{\varepsilon}_1, \dot{\varepsilon}_2, \theta')_{ss1} = (\dot{\gamma}/2, -\dot{\gamma}/2, 0), \quad (2)$$

where the stress loading orientation angle θ is defined as the angle between σ_1 and the rolling direction of the sheet metal with $\sigma_1 \geq \sigma_2$ [17, 19]. The plastic strain increment loading orientation angle θ' is defined as the angle between $\dot{\varepsilon}_1$ and the rolling direction of the sheet metal with $\dot{\varepsilon}_1 \geq \dot{\varepsilon}_2$.

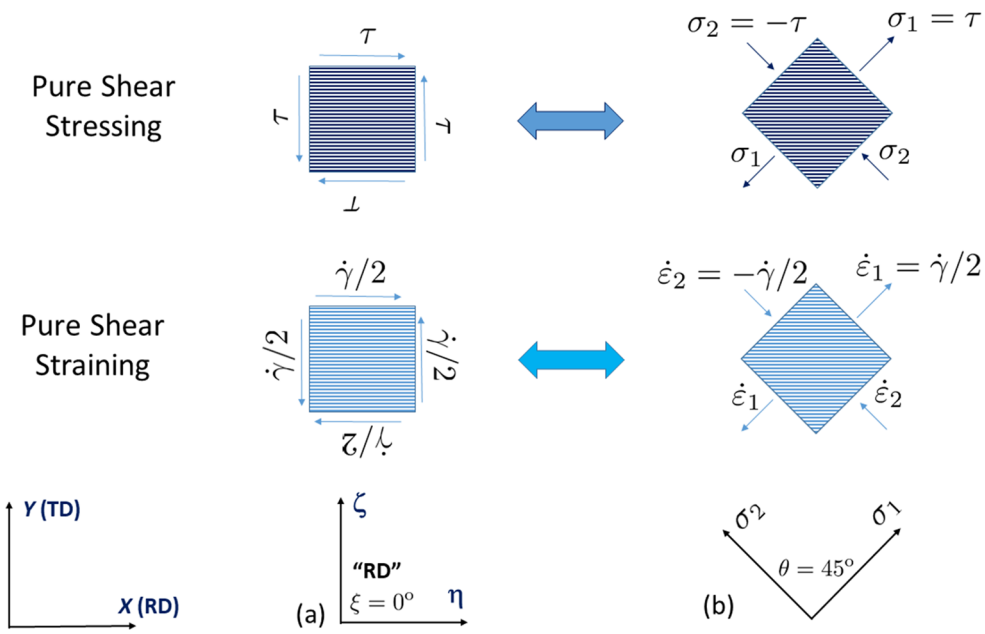

Fig. 3 Pure shear stressing and straining of a sheet metal with 0-degree parallel to its material coordinates xy: **a** the RD material element edges aligned with the laboratory (shearing) coordinates $\eta\zeta$; **b** the material element edges aligned with principal stress axes $\sigma_1\sigma_2$

In general $\theta' \neq \theta$ but here $\theta' = \theta = 0$ is always held for the *on-axis* pure shear (but $\xi = 45^o$!). The subscripts"ps1" and "ss1" are used to designate the first case of the pure shear stressing and straining conditions respectively.

0-degree parallel shearing $\xi = 0^o$ (special off-axis loading $\theta = \theta' = 45^o$)

As shown in Fig. 3(a), either pure shear stressing or straining may be applied to a square unit material element aligned with the rolling direction (x-axis) of the sheet metal (the RD shear test sample). They shall be called 0-degree parallel shearing loading conditions and may be described in terms of the unit material element aligned with the principal stress axes shown in Fig. 3(b) as well. Using the Cartesian components in the sheet metal material symmetry coordinate system (at a 45-degree angle clockwise from the principal stress axes), the pure shear yield stress and plastic strain increment tensors shown in Fig. 3(a) are given respectively as

$$(\sigma_x, \sigma_y, \tau_{xy})_{ps2} = (0, 0, \tau), \quad (\dot\varepsilon_x, \dot\varepsilon_y, \dot\varepsilon_{xy})_{ss2} = (0, 0, \dot\gamma/2). \tag{3}$$

The corresponding representation of the same pure shear stressing and straining conditions in terms of the principal stresses and plastic strain increments shown in Fig. 3(b) are given respectively as

$$(\sigma_1, \sigma_2, \theta)_{ps2} = (\tau, -\tau, 45^o), \quad (\dot\varepsilon_1, \dot\varepsilon_2, \theta')_{ss2} = (\dot\gamma/2, -\dot\gamma/2, 45^o). \tag{4}$$

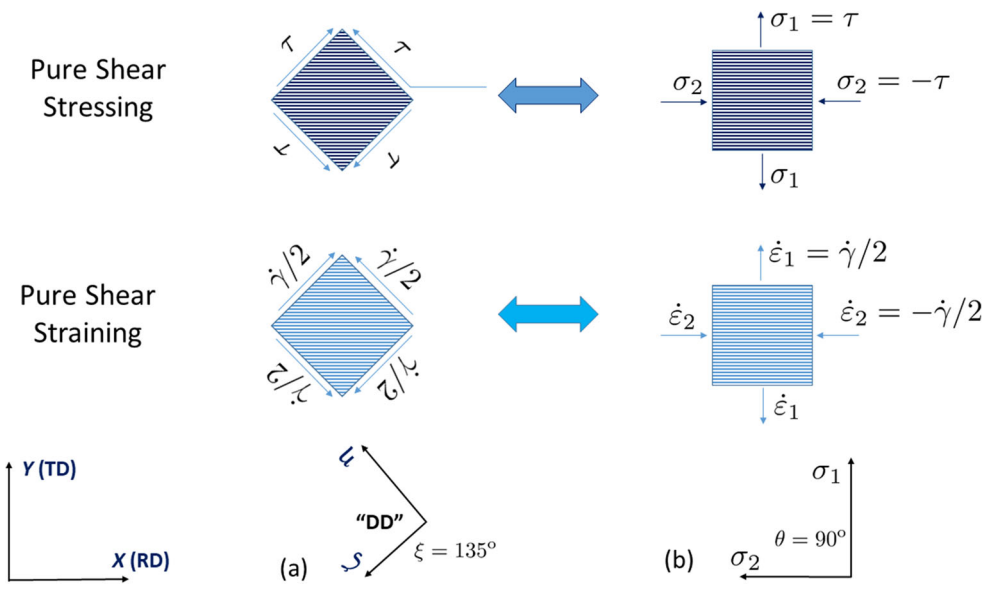

Fig. 4 Pure shear stressing and straining of a sheet metal at 135-degree diagonal to its material coordinates xy: **a** the DD material element edges aligned with the laboratory (shearing) coordinates $\eta\zeta$; **b** the material element edges aligned with principal stress axes $\sigma_1\sigma_2$

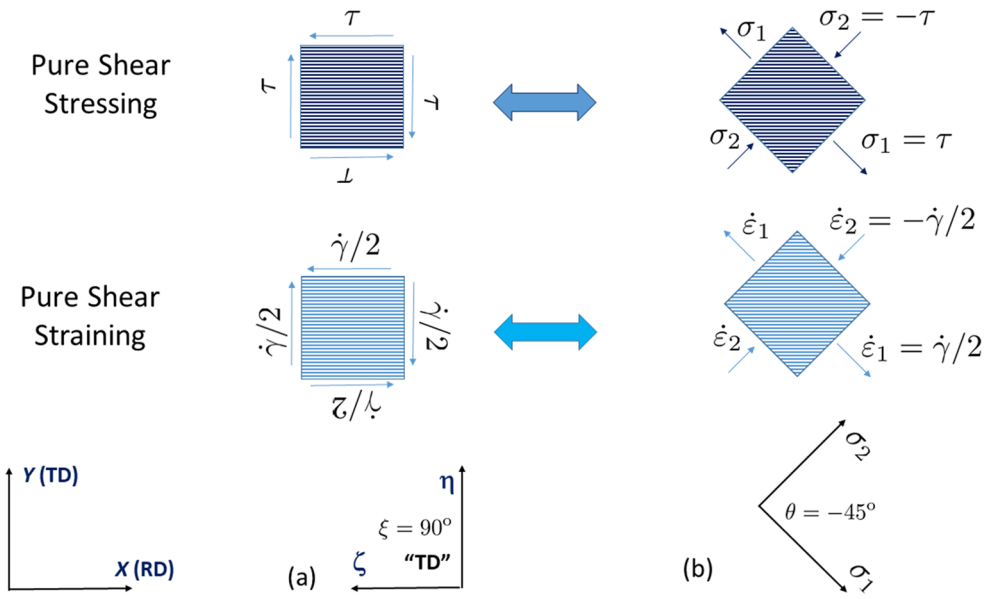

Fig. 5 Pure shear stressing and straining of a sheet metal with 90-deg or perpendicular to its material coordinates xy: **a** the TD material element edges aligned with the laboratory (shearing) coordinates $\eta\zeta$; **b** the material element edges aligned with principal stress axes $\sigma_1\sigma_2$.

135-degree diagonal shearing $\xi = 135^o$ (on-axis loading $\theta = \theta' = 90^o$)

When the shear stress or plastic shear strain increments are applied in the opposite directions to a square unit material element shown in Fig. 2(a), the pure shear loading condition will be called 135-degree diagonal shearing, see Fig. 4(a). The corresponding stressing and straining conditions in terms of the unit material element aligned along the principal stress axes are shown in Fig. 4(b) which are the ones shown in Fig. 2(b) rotated counterclockwise by 90-degree. The pure shear stress and strain increment tensors shown in Fig. 4(a) are given respectively in terms of the Cartesian components in the sheet metal material symmetry coordinate system as

$$(\sigma_x, \sigma_y, \tau_{xy})_{ps3} = (-\tau, \tau, 0), \quad (\dot{\varepsilon}_x, \dot{\varepsilon}_y, \dot{\varepsilon}_{xy})_{ss3} = (-\dot{\gamma}/2, \dot{\gamma}/2, 0). \quad (5)$$

The same pure shear stress and plastic strain increment tensors in terms of the principal stresses and strain increments shown in Fig. 4(b) are given respectively as

$$(\sigma_1, \sigma_2, \theta)_{ps3} = (\tau, -\tau, 90^o), \quad (\dot{\varepsilon}_1, \dot{\varepsilon}_2, \theta')_{ss3} = (\dot{\gamma}/2, -\dot{\gamma}/2, 90^o). \quad (6)$$

90-degree perpendicular shearing $\xi = 90^o$ (special off-axis loading $\theta = \theta' = -45^o$)

For the completeness, we also consider the case of 90-degree parallel shearing shown in Fig. 5(a), that is, the square unit material element under shearing is aligned with the transverse direction (y-axis) of the sheet metal (the TD shear test sample). The pure shear stress and plastic strain increment tensors shown in Fig. 5(a) are given respectively in terms of the Cartesian components in the sheet metal material symmetry coordinate system (at a 45-degree angle clockwise from the principal stress axes) as

$$(\sigma_x, \sigma_y, \tau_{xy})_{ps4} = (0, 0, -\tau), \quad (\dot{\varepsilon}_x, \dot{\varepsilon}_y, \dot{\varepsilon}_{xy})_{ss4} = (0, 0, -\dot{\gamma}/2). \quad (7)$$

The corresponding representation of the same pure shear loading conditions in terms of the principal stresses and plastic strain increments shown in Fig. 5(b) are given respectively as

$$(\sigma_1, \sigma_2, \theta)_{ps4} = (\tau, -\tau, -45^o), \quad (\dot{\varepsilon}_1, \dot{\varepsilon}_2, \theta')_{ss4} = (\dot{\gamma}/2, -\dot{\gamma}/2, -45^o). \quad (8)$$

Modeling Pure Shear by Hill's Quadratic and Gotoh's Quartic Anisotropic Plastic Models

We are now ready to compute the plastic strain increments from an applied pure shear yield stress and to evaluate the yield stress components from an applied simple shear plastic strain increment for four shearing loading cases detailed in the previous section. More specifically, we seek after the ratio of principal strain increments $\dot{\varepsilon}_2/\dot{\varepsilon}_1$ per pure shear in stress and the ratio of principal stresses σ_2/σ_1 per simple shear or pure shear in strain as predicted by Hill's quadratic yield/flow functions and Gotoh's quartic yield function given in Appendix.

Principal Plastic Strain Increment Ratio in Pure Shear Stressing

Per the yield functions and flow rule $\dot{\boldsymbol{\varepsilon}}^p = \lambda \partial g/\partial \boldsymbol{\sigma}$ given in Appendix, the plastic strain increments are readily

computed in terms of the three stress components in the sheet metal material symmetry coordinate system as

$$\dot{\varepsilon}_x = \lambda \partial g/\partial \sigma_x, \quad \dot{\varepsilon}_y = \lambda \partial g/\partial \sigma_y, \quad \dot{\gamma}_{xy} = 2\dot{\varepsilon}_{xy} = \lambda \partial g/\partial \tau_{xy}. \tag{9}$$

For an associated Hill's quadratic model ($g^2 = \Phi_{2y}$), the plastic strain increments for the four pure shear plane-stress states given by Eqs. $(1)_1$, $(3)_1$, $(5)_1$ and $(7)_1$ are (the common factor $\lambda\tau/(2g)$ is dropped for simplicity)

$$\begin{aligned}
&(\dot{\varepsilon}_x, \dot{\varepsilon}_y, \dot{\varepsilon}_{xy})^h_{ps1} \propto (2Y_1 - Y_2, Y_2 - 2Y_3, 0),\\
&(\dot{\varepsilon}_x, \dot{\varepsilon}_y, \dot{\varepsilon}_{xy})^h_{ps2} \propto (0, 0, Y_4),\\
&(\dot{\varepsilon}_x, \dot{\varepsilon}_y, \dot{\varepsilon}_{xy})^h_{ps3} \propto (-2Y_1 + Y_2, -Y_2 + 2Y_3, 0),\\
&(\dot{\varepsilon}_x, \dot{\varepsilon}_y, \dot{\varepsilon}_{xy})^h_{ps4} \propto (0, 0, -Y_4),
\end{aligned} \tag{10}$$

The corresponding principal plastic strain increments and straining orientation angle are

$$\begin{aligned}
&(\dot{\varepsilon}_1, \dot{\varepsilon}_2, \theta')^h_{ps1} \propto (2Y_1 - Y_2, Y_2 - 2Y_3, 0),\\
&(\dot{\varepsilon}_1, \dot{\varepsilon}_2, \theta')^h_{ps2} \propto (Y_4, -Y_4, 45^o),\\
&(\dot{\varepsilon}_1, \dot{\varepsilon}_2, \theta')^h_{ps3} \propto (-Y_2 + 2Y_3, -2Y_1 + Y_2, 90^o),\\
&(\dot{\varepsilon}_1, \dot{\varepsilon}_2, \theta')^h_{ps4} \propto (Y_4, -Y_4, -45^o),
\end{aligned} \tag{11}$$

In the case of using a non-associated Hill's model ($g^2 = \Phi_{2p}$), the above results are still applied with material constants (Y_1, Y_2, Y_3, Y_4) being replaced by material constants (P_1, P_2, P_3, P_4).

For an associated Gotoh's quartic model ($g^4 = \Phi_4$), the plastic strain increments for the same four pure shear loading cases are computed straightforward as (the common factor $\lambda\tau^3/(4g^3)$ is dropped for simplicity)

$$\begin{aligned}
&(\dot{\varepsilon}_x, \dot{\varepsilon}_y, \dot{\varepsilon}_{xy})^g_{ps1} \propto (4A_1 - 3A_2 + 2A_3 - A_4, A_2 - 2A_3 + 3A_4 - 4A_5, 0),\\
&(\dot{\varepsilon}_x, \dot{\varepsilon}_y, \dot{\varepsilon}_{xy})^g_{ps2} \propto (0, 0, 2A_9),\\
&(\dot{\varepsilon}_x, \dot{\varepsilon}_y, \dot{\varepsilon}_{xy})^g_{ps3} \propto (-4A_1 + 3A_2 - 2A_3 + A_4, -A_2 + 2A_3 - 3A_4 + 4A_5, 0),\\
&(\dot{\varepsilon}_x, \dot{\varepsilon}_y, \dot{\varepsilon}_{xy})^g_{ps4} \propto (0, 0, -2A_9),
\end{aligned} \tag{12}$$

The corresponding principal plastic strain increments and straining orientation angle are

$$\begin{aligned}
&(\dot{\varepsilon}_1, \dot{\varepsilon}_2, \theta')^g_{ps1} \propto (4A_1 - 3A_2 + 2A_3 - A_4, A_2 - 2A_3 + 3A_4 - 4A_5, 0),\\
&(\dot{\varepsilon}_1, \dot{\varepsilon}_2, \theta')^g_{ps2} \propto (2A_9, -2A_9, 45^o),\\
&(\dot{\varepsilon}_1, \dot{\varepsilon}_2, \theta')^g_{ps3} \propto (-A_2 + 2A_3 - 3A_4 + 4A_5, -4A_1 + 3A_2 - 2A_3 + A_4, 90^o),\\
&(\dot{\varepsilon}_1, \dot{\varepsilon}_2, \theta')^g_{ps4} \propto (2A_9, -2A_9, -45^o).
\end{aligned} \tag{13}$$

Principal stress ratio in pure shear straining

When the plastic loading condition is imposed by prescribing all plastic strain increment components (consistent with the plastic incompressibility), the corresponding yield stress components may be computed from both the flow rule and yield condition. As we are mostly interested in the principal stress ratio in simple shear straining, only the relative values among the stress components (σ_x, σ_y, τ_{xy}) are first sought from the given plastic strain increments ($\dot{\varepsilon}_x$, $\dot{\varepsilon}_y$, $\dot{\varepsilon}_{xy}$).

One can show that the associated Hill's quadratic model gives the following Cartesian components of strain increments in terms of stresses for the four simple shear straining conditions defined by Eqs. $(1)_2$, $(3)_2$,$(5)_2$ and $(7)_2$ (again any common factor is dropped for simplicity)

$$\begin{aligned}
&(2Y_1\sigma_x + Y_2\sigma_y, Y_2\sigma_x + 2Y_3\sigma_y, Y_4\tau_{xy})^h_{ss1} \propto (\dot{\gamma}/2, -\dot{\gamma}/2, 0),\\
&(2Y_1\sigma_x + Y_2\sigma_y, Y_2\sigma_x + 2Y_3\sigma_y, Y_4\tau_{xy})^h_{ss2} \propto (0, 0, \dot{\gamma}),\\
&(2Y_1\sigma_x + Y_2\sigma_y, Y_2\sigma_x + 2Y_3\sigma_y, Y_4\tau_{xy})^h_{ss3} \propto (-\dot{\gamma}/2, \dot{\gamma}/2, 0),\\
&(2Y_1\sigma_x + Y_2\sigma_y, Y_2\sigma_x + 2Y_3\sigma_y, Y_4\tau_{xy})^h_{ss4} \propto (0, 0, -\dot{\gamma}).
\end{aligned} \tag{14}$$

One can thus obtain the corresponding principal stress ratio for each case as

$$\begin{aligned}
&(\sigma_1, \sigma_2, \theta)^h_{ss1} = (\sigma_x, \sigma_y, 0): \quad (\frac{\sigma_2}{\sigma_1})^h_{ss1} = -\frac{2Y_1 + Y_2}{Y_2 + 2Y_3};\\
&(\sigma_1, \sigma_2, \theta)^h_{ss2} = (\tau_{xy}, -\tau_{xy}, 45^o): \quad (\frac{\sigma_2}{\sigma_1})^h_{ss2} = -1;\\
&(\sigma_1, \sigma_2, \theta)^h_{ss3} = (\sigma_y, \sigma_x, 90^o): \quad (\frac{\sigma_2}{\sigma_1})^h_{ss3} = -\frac{Y_2 + 2Y_3}{2Y_1 + Y_2};\\
&(\sigma_1, \sigma_2, \theta)^h_{ss4} = (\tau_{xy}, -\tau_{xy}, -45^o): \quad (\frac{\sigma_2}{\sigma_1})^h_{ss4} = -1.
\end{aligned} \tag{15}$$

Again, the above results are applied to a non-associated Hill's model too with material constants (Y_1, Y_2, Y_3, Y_4) being replaced by (P_1, P_2, P_3, P_4).

Recall from the associated flow rule, the Gotoh's quartic model gives the plastic strain increments in plane-stress as (without any common factor for simplicity)

$$\begin{aligned}
&\dot{\varepsilon}_x \propto 4A_1\sigma_x^3 + 3A_2\sigma_x^2\sigma_y + 2A_3\sigma_x\sigma_y^2 + A_4\sigma_y^3 + 2A_6\sigma_x\tau_{xy}^2 + A_7\sigma_y\tau_{xy}^2,\\
&\dot{\varepsilon}_y \propto A_2\sigma_x^3 + 2A_3\sigma_x^2\sigma_y + 3A_4\sigma_x\sigma_y^2 + 4A_5\sigma_y^3 + A_7\sigma_x\tau_{xy}^2 + 2A_8\sigma_y\tau_{xy}^2,\\
&2\dot{\varepsilon}_{xy} = \dot{\gamma}_{xy} \propto A_6\sigma_x^2\tau_{xy} + A_7\sigma_x\sigma_y\tau_{xy} + A_8\sigma_y^2\tau_{xy} + 2A_9\tau_{xy}^3.
\end{aligned} \tag{16}$$

For the same four simple shear straining conditions defined by Eqs. $(1)_2$, $(3)_2$, $(5)_2$ and $(7)_2$, one has the following plane-stress results

$$\begin{aligned}
&(\sigma_1, \sigma_2, \theta)^g_{ss1} = (\sigma_x, \sigma_y, 0):\\
&\quad 4A_1 + (3\kappa_1 + 1)A_2 + 2(\kappa_1^2 + \kappa_1)A_3 + (\kappa_1^3 + 3\kappa_1^2)A_4 + 4\kappa_1^3 A_5 = 0;\\
&(\sigma_1, \sigma_2, \theta)^g_{ss2} = (\tau_{xy}, -\tau_{xy}, 45^o): \quad (\frac{\sigma_2}{\sigma_1})^g_{ss2} = -1;\\
&(\sigma_1, \sigma_2, \theta)^g_{ss3} = (\sigma_y, \sigma_x, 0):\\
&\quad 4\kappa_2^3 A_1 + (3\kappa_2^2 + \kappa_2^3)A_2 + 2(\kappa_2 + \kappa_2^2)A_3 + (1 + 3\kappa_2)A_4 + 4A_5 = 0;\\
&(\sigma_1, \sigma_2, \theta)^g_{ss4} = (\tau_{xy}, -\tau_{xy}, -45^o): \quad (\frac{\sigma_2}{\sigma_1})^g_{ss4} = -1;
\end{aligned} \tag{17}$$

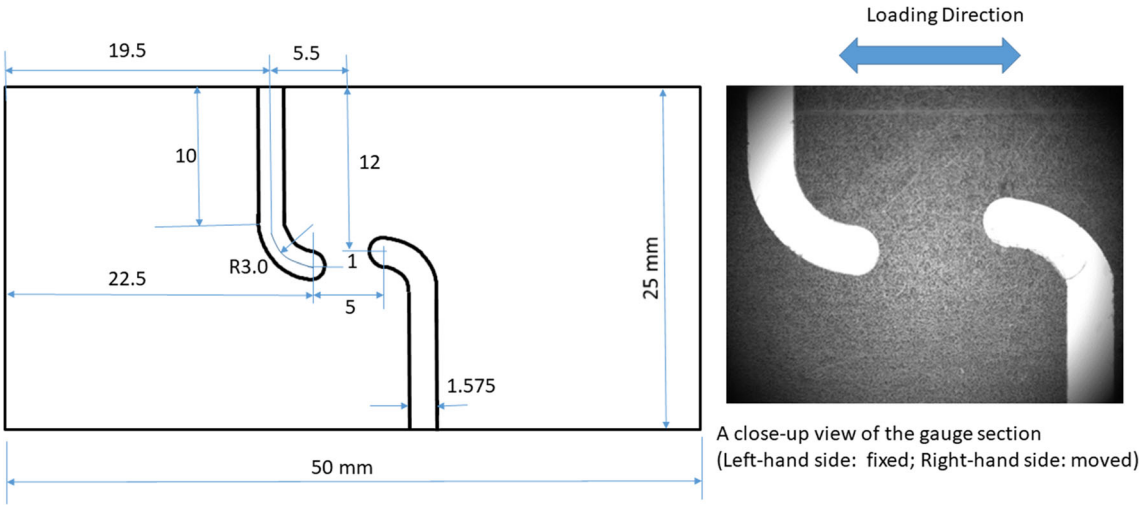

Fig. 6 Dimensions of Type A shearing test coupon and a close-up view image of an as-machined AA6111-T4 sheet sample with a thickness of 1.2mm

where $\kappa_1 = (\frac{\sigma_2}{\sigma_1})^g_{ss1}$ and $\kappa_2 = (\frac{\sigma_2}{\sigma_1})^g_{ss3}$ are principal stress ratios given by Gotoh's yield function in simple shear loading cases #1 and #3 and they may be solved per a cubic algebraic equation for the known material constants $(A_1, A_2, A_3, A_4, A_5)$ of a given sheet metal.

Shearing Experiments and Results on an AA6111-T4 Sheet

It is important to note that the origin of the newly proposed shear constraint by Abedini et al. [2] was motivated in part in their effort to incorporate shearing test results into the calibration of an anisotropic yield function. Here we present some shearing experiments of our own on an AA6111-T4 sheet with two different test coupon designs. Shearing test results from our experiments were shown to highlight the difference between the idealized pure shear loading conditions and deformation states described in Section Modeling Pure Shear by Hill's Quadratic and Gotoh's Quartic Anisotropic Plastic Models and the actual loading conditions and deformation states obtained in practice in a shearing test used for sheet metals.

Two sheet metal shearing tests using a universal materials testing machine

Due to their comparative simplicity, shearing tests of a sheet metal are most commonly carried out using specially designed test coupons loaded in tension on a universal materials test machine [8, 12, 22, 25, 29, 30]. Two of the shear test coupon designs without the need of removing any surface layer of the sheet metal were considered in this study: Type A as shown in Fig. 6 per [2, 29] and Type B as shown in Fig. 7 per [1, 10]. The actual dimensions of each test coupon geometry used in this study

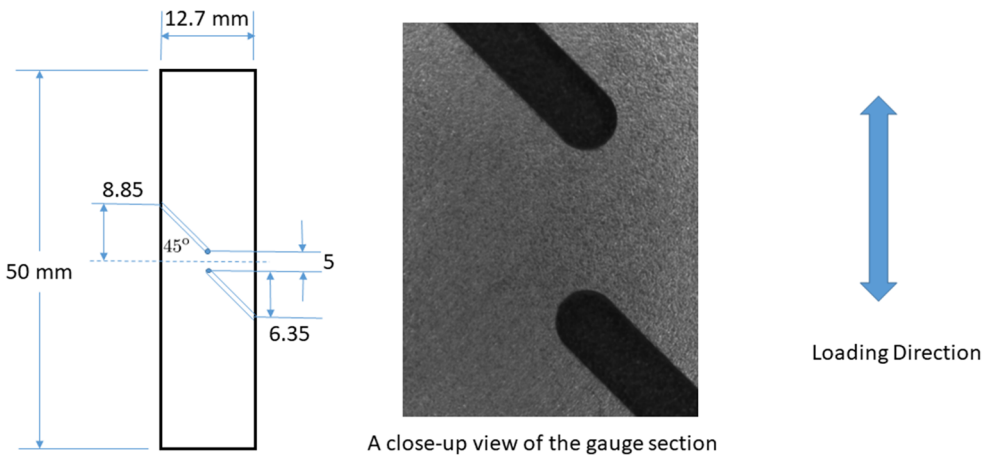

Fig. 7 Dimensions of Type B shearing test coupon and a close-up view image of an as-machined AA6111-T4 sheet sample with a thickness of 1.2mm

are given in mm in each figure. Each shear test coupon was cut from an aluminum alloy sheet metal AA6111-T4 of 1.2mm in thickness on a CNC machine using an end mill of 0.062 inch in diameter. A digital image of a close-up view of the shearing zone of each as-machined AA6111-T4 sheet test coupon is shown as an insert in each figure. The representative tensile properties of the aluminum sheet metal have been reported elsewhere [41]. The yield stresses and plastic strain ratios from three standard uniaxial tension tests on AA6111-T4 sheet used in this study are $(\sigma_0, \sigma_{45}, \sigma_{90}) = (174.1, 173.4, 166.7)$ MPa and (R_0, R_{45}, R_{90})=(0.93,0.41,0.66).

The shearing experiments using Type A and Type B test coupons were carried out in the displacement control mode on an Instron 5967 universal materials test machine with a 30 kN static load cell. A constant cross-head speed of 1.8 mm/min was used in all experiments. A pair of RD and DD samples of Type A and Type B coupons were tested. They consist of samples subjected to the tensile loading along the RD and along the DD or 45-degree from the RD of the sheet metal respectively. Each test coupon was held at both ends by a pair of wedge grips with flat but serrated faces and was tension loaded to final fracture while the upper cross-head displacement and load cell readings were recorded continuously at 100 Hz data acquisition rate. During each shearing test, a monochrome digital CCD camera from Point Grey Research Inc. (www.ptgrey.com) with a zoom lens was used to image one surface of the shearing zone of the test sample at 1 frame per second. A total of about 100 images were acquired for each test. Each image has a size of 3376-by-2704 pixels with a typical pixel resolution around 2.7 microns/pixel. Whole-field strain maps of the sheared samples at various deformation stages up to the maximum load level were obtained by digital image correlation (DIC) of in-situ acquired sample images based on the Lucas-Kanade inverse compositional algorithm [7, 28, 31]. At

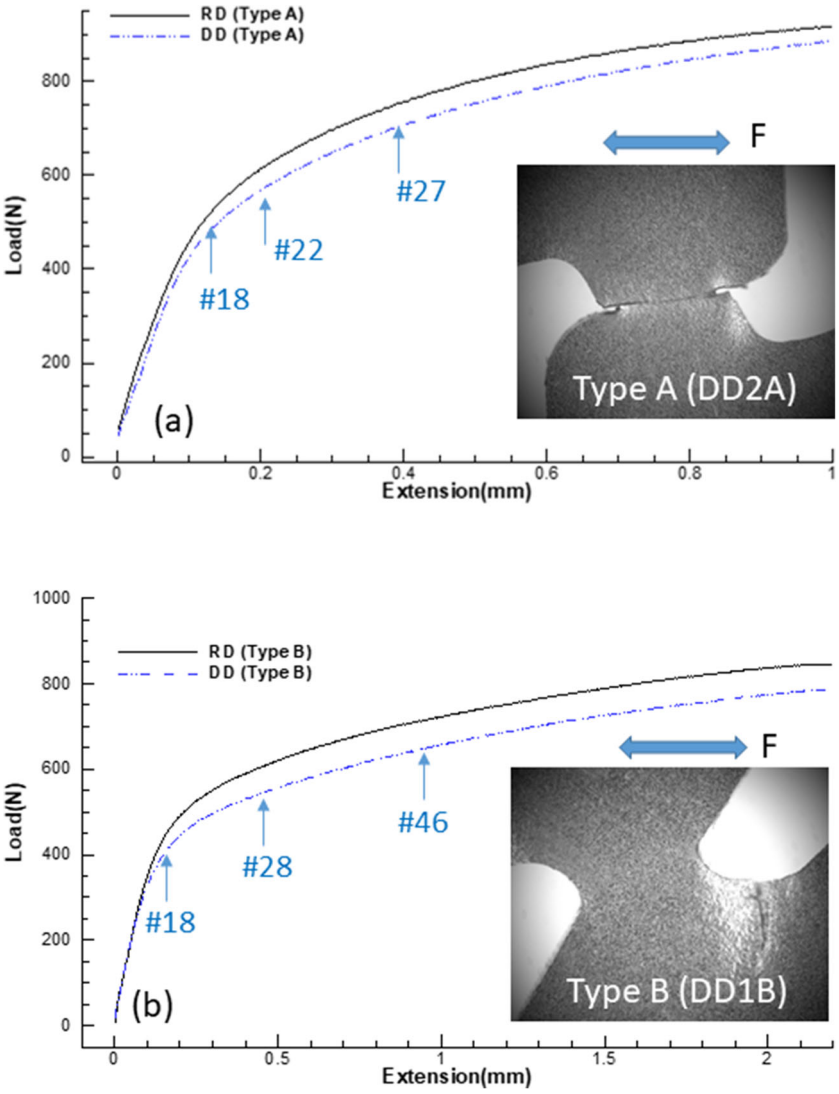

Fig. 8 The load versus displacement data from four shearing tests on AA6111-T4 sheet: **a** two Type A samples RD2A and DD2A; **b** two Type B samples RD1B and DD1B. Frame numbers of three representative images recorded for DD2A and DD1B samples are also marked at their corresponding load and displacement levels. Images of shear test samples DD2A and DD1B after fracture are also inserted here

this particular magnification of the experiments, the natural contrast pattern on the surface of as-received aluminum sheet metals was used for the image-based deformation analysis (i.e., no sprayed paint droplets or ink marks were ever applied to the sample surfaces). A typical local DIC analysis used a subset of 61-by-61 pixels over 5-by-5 pixel grid spacing. The average displacement gradients were computed over each subset to obtain its local logarithmic strains commonly used in metal plasticity. For a few images at the very initial stage of each test, a large subset up to twice as big was used to reduce the noise levels in the local strain mapping data.

Experimental Results

The measured tensile load versus the cross-head displacement data for shearing tests of the two Type A samples (RD2A and DD2A) are shown in Fig. 8(a). There is a significant difference between the RD2A and DD2A samples, reflecting the plastic anisotropy of the material. As shown in Fig. 8(b), a similar difference between the RD1B and DD1B samples of Type B was also observed in the measured tensile load versus the cross-head displacement data. That is, the load levels of the DD samples of both Type A and Type B at a given displacement were found to be lower than those of the RD samples. Also shown in Fig. 8(a) and (b) are the images of the fractured shear test samples DD2A and DD1B. Unlike the Type A samples that failed in shear right at the gauge zone, all Type B samples failed due to the tensile fracture at the location far away from the initial shearing zone (noting the applied loading direction for both samples in Fig. 8(a) and (b) is horizontal).

Following the usual practice [2, 10, 29], one may obtain the nominal shear stress-strain curves ($\tau_{\eta\zeta}$ vs $\gamma_{\eta\zeta}$) for these four shear tests. The initial portion of their shear stress-strain curves up to shear strain $\gamma_{\eta\zeta} = 0.24$ is shown in Fig. 9. Here the shear stress is the average shear stress over the cross-section across the narrowest width (along the horizontal tensile direction or η-axis) of the shearing zone in each sample. That is, $\tau_{\eta\zeta} = F_\eta/A_0 = F_\eta/(w_0 t_0)$, where F_η is the applied tensile force at the two ends of each shear sample and w_0 and t_0 are the initial width and thickness of the *out-of-plane* shearing zone cross-section. In our study here, w_0=3.568mm and 3.425mm respectively for Type A and Type B samples and $t_0 = 1.2$mm (so the aspect ratio of the shearing zone cross-section is about 3). The shear strain $\gamma_{\eta\zeta}$ is the average of the local (logarithmic) shear strains obtained by the digital image correlation over the *in-plane* narrow rectangular region of the shearing zone in each sample. The region for computing the average shear strain is shown as a white horizontal rectangle on the image inserts of Fig. 9 for a Type A sample DD2A and a Type B sample DD1B. The vertical height of the region h_0 is chosen to be about 0.350-0.375 mm (so the aspect ratio of the in-plane local rectangular gauge section is about 10). If one assumes that the shearing zone of each sample is under predominantly pure shear stressing loading initially (i.e., neglecting any in-plane normal stresses σ_η and σ_ζ), then the loading angle θ is thus approximately to be 45° for RD samples and 0° for DD samples (see Section Two Types of Pure Shear Loading Conditions on a Sheet Metal for details). The initial yield stresses were obtained by a large offset method as $\sigma_{s45} = 116.8$ MPa and 113.1 MPa for the two RD samples (RD2A and RD1B) and as $\sigma_{s0} =$

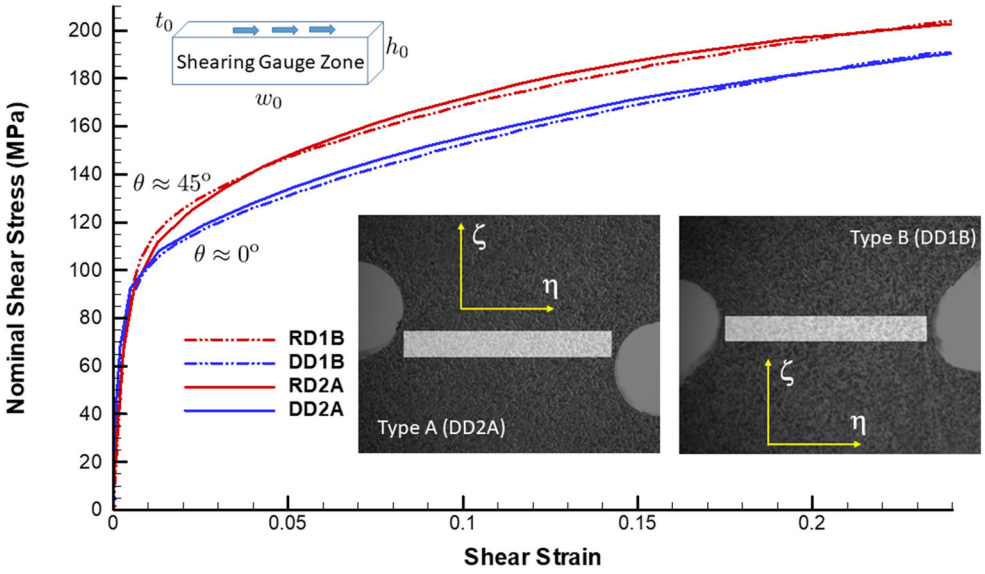

Fig. 9 The nominal shear stress $\tau_{\eta\zeta}$ versus shear strain $\gamma_{\eta\zeta}$ curves from the four shearing tests on AA6111-T4 sheet. The laboratory loading and measurement coordinates $\eta\zeta$ are shown in the image inserts of two selected samples DD2A and DD1B. A 3D schematic of the nominal shearing gauge zone with its width w_0, height h_0 and thickness t_0 is also given

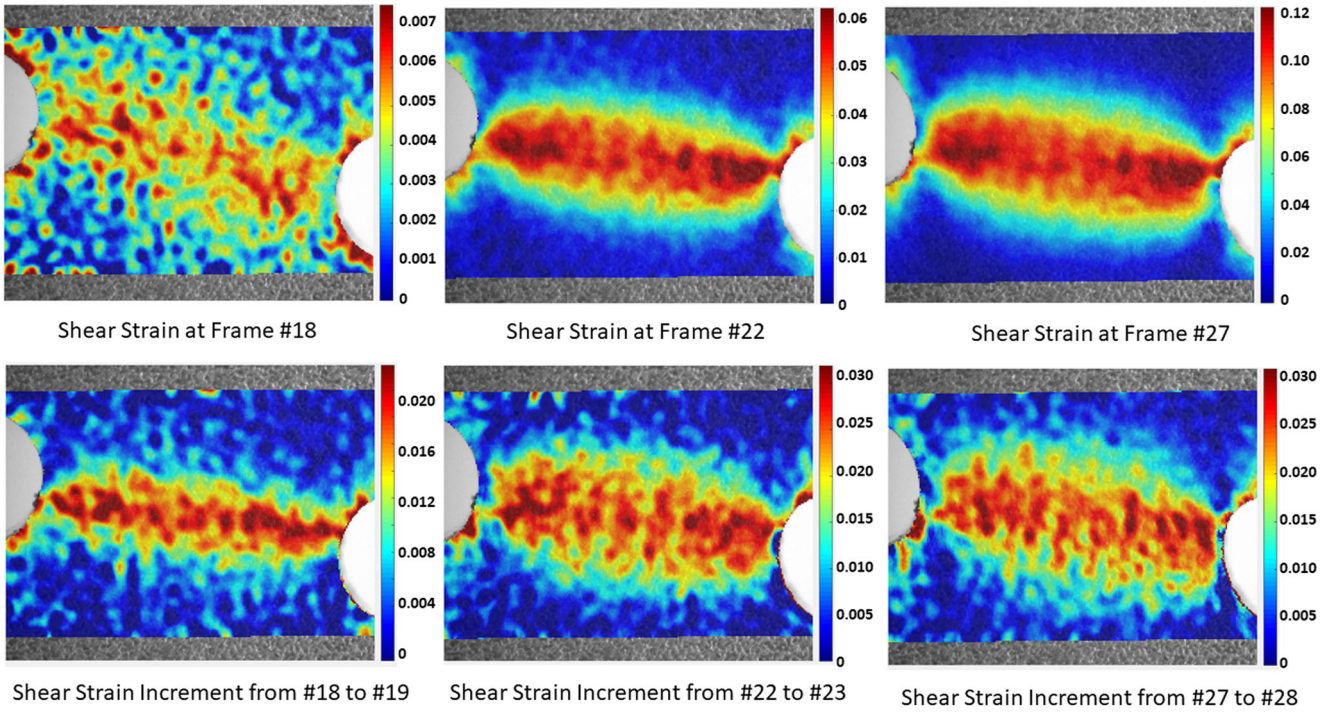

Fig. 10 The total shear strain $\gamma_{\eta\zeta}$ maps obtained from a digital image correlation analysis of image frame numbers 18, 22 and 27 for the shearing test sample DD2A. The corresponding incremental shear strain $\Delta\gamma_{\eta\zeta}$ maps obtained from a digital image correlation analysis of image pairs 18-19, 22-23 and 27-28 are also shown in the lower half of the figure

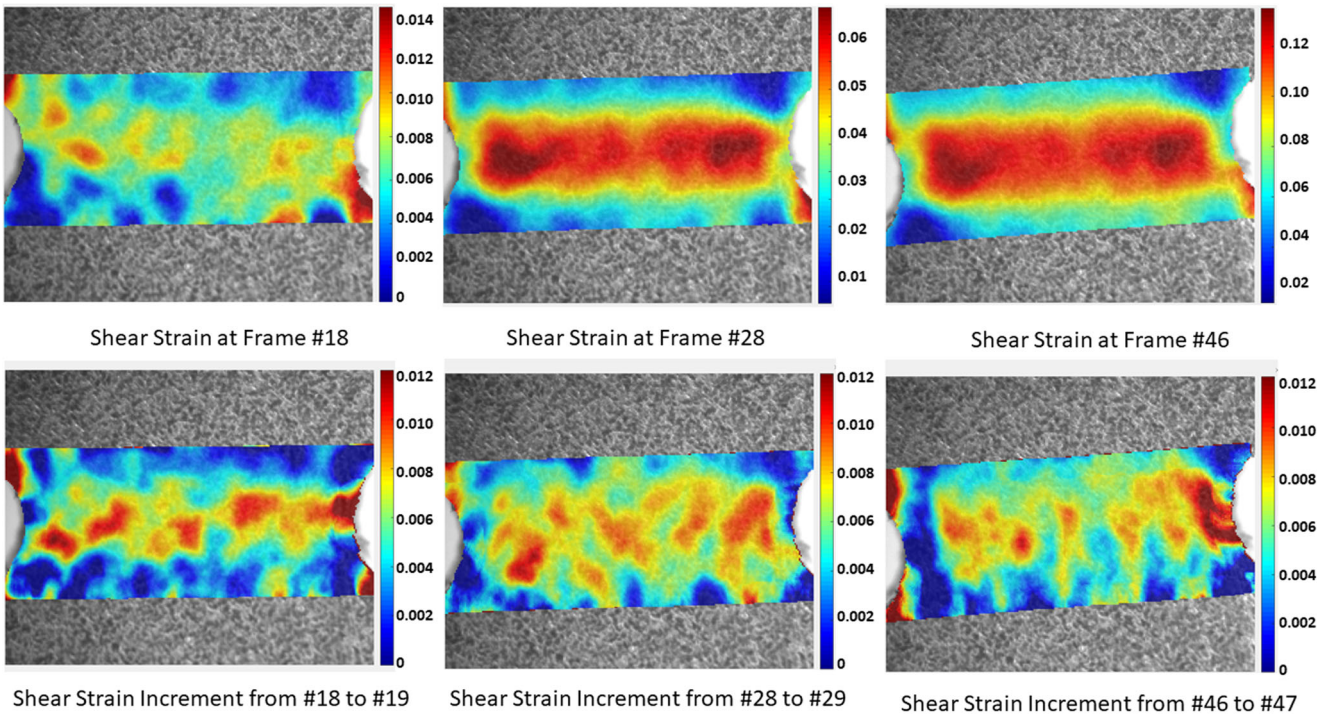

Fig. 11 The total shear strain $\gamma_{\eta\zeta}$ maps obtained from a digital image correlation analysis of image frame numbers 18, 28 and 46 for the shearing test sample DD1B. The corresponding incremental shear strain $\Delta\gamma_{\eta\zeta}$ maps obtained from a digital image correlation analysis of image pairs 18-19, 28-29 and 46-47 are also shown in the lower half of the figure

104.8 MPa and 105.4 MPa for the two DD samples (DD2A and DD1B).

The actual state of the in-plane surface deformation inside the shearing gauge zone (w_0-by-h_0) and its surrounding regions of the two shearing test samples DD2A and DD1B in terms of total and incremental shear strain maps are shown in Figs. 10 and 11 respectively for three selective load and deformation levels. Frame numbers of the images at those load and displacement levels during the tests of DD2A and DD1B samples are indicated in Fig. 8(a) and (b). Those images approximately correspond to the average shear strains $\gamma_{\eta\zeta}$= 0.01, 0.05 and 0.1 of Fig. 9. Also shown in both Figs. 10 and 11 are the incremental shear strain maps for these two shearing test samples around those three load levels. Because the images were recorded at a frame rate of 1 frame per second in the tests, these incremental shear strain maps may be regarded approximately as the local shear strain rates of the test samples. Clearly, a straight line cutting through the narrow shearing zone (i.e., the high shear strain strip) in each test sample is not parallel to the horizontal tensile loading direction at all. The angles between the active shearing zone in terms of the incremental shear strain maps in Figs. 10 and 11 and the horizontal direction is about $6-8^{o}$ for DD2A sample and $5-7^{o}$ for DD1B sample.

The nature of the in-plane deformation of the shearing zone and its surrounding regions can be further illustrated by additional maps for DD2A and DD1B samples. Maps of the sum of the two principal strains $\varepsilon_1+\varepsilon_2$, the angle of the current principal shearing plane ϕ_s, and the angle of in-plane rigid-body rotation ω due to shearing are shown in Fig. 12 for DD2A sample at load steps corresponding to image frames No.22 and No.27. Even at the interior center region of the shearing zone excluding the two regions near free edges, the average local $\varepsilon_1+\varepsilon_2$ is found to be as high as -0.009 and -0.014 (noting $\varepsilon_1-\varepsilon_2$ is about 0.05 and 0.1). The angle of the current principal shearing plane and the horizontal direction is about 4.5^{o} and 7^{o} at these two load steps. On the other hand, the rigid-body rotation due to shearing is only about 2.1^{o} and 4.5^{o} (counterclockwise).

Similarly, maps of the sum of the two principal strains $\varepsilon_1+\varepsilon_2$, the angle of the current principal shearing plane ϕ_s, and the angle of in-plane rigid-body rotation ω due to shearing are shown in Fig. 13 for DD1B sample at load steps corresponding to image frames No.28 and No.46. At the interior center region of the shearing zone, the average local

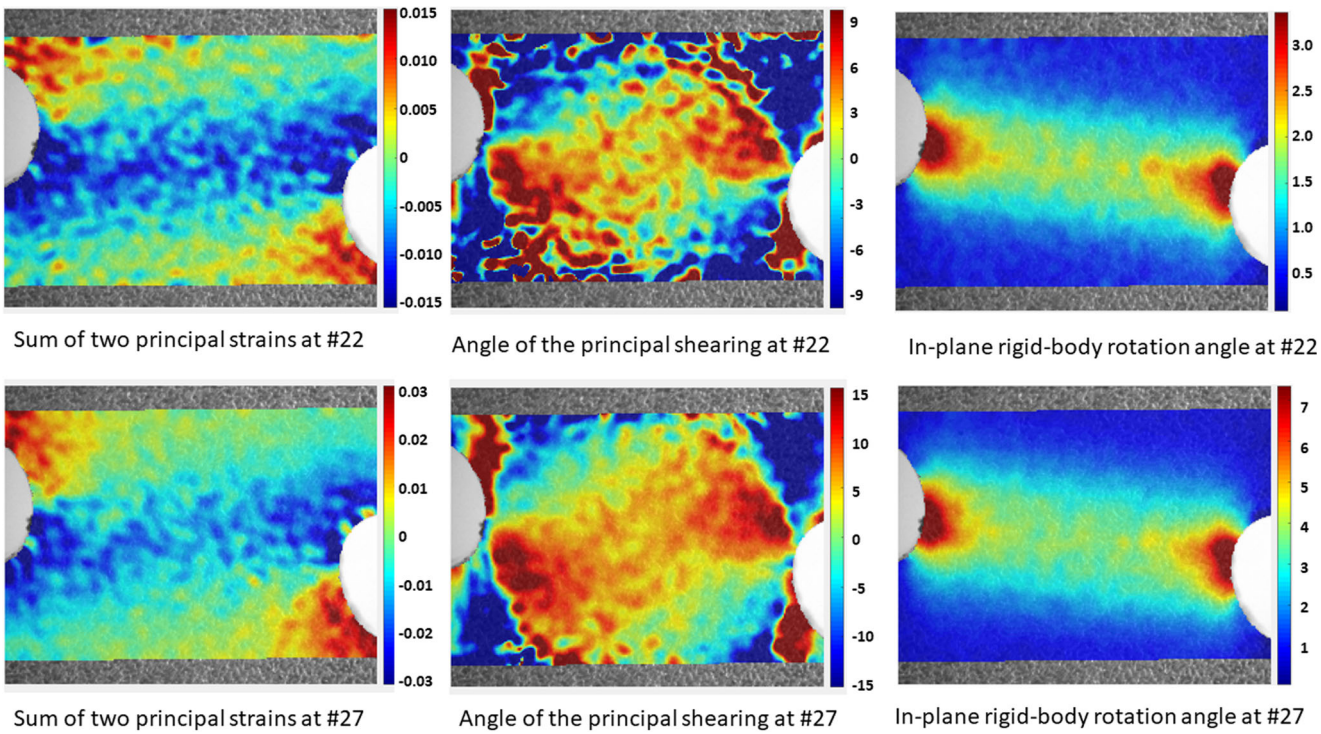

Fig. 12 Three additional maps from the whole-field strain measurements for DD2A sample from image frame No.22 and No.27: **a** the sum of two in-plane principal strains (left); **b** the angle in degree of the principal shearing plane deviating from the horizontal direction (middle); **c** the angle in degree of the in-plane rigid-body rotation due to shearing (right)

$\varepsilon_1 + \varepsilon_2$ is found to be smaller values of -0.005 and -0.003 (noting $\varepsilon_1 - \varepsilon_2$ is again about 0.05 and 0.1). The angle of the current principal shearing plane and the horizontal direction is 4° and 1° at these two load steps. On the other hand, the rigid-body rotation due to shearing is only about 3.5° and 8° (counterclockwise).

Discussion and Conclusions

Calibrated Hill's and Gotoh's yield functions for AA6111-T4 sheet

When a total of seven experimental inputs ($\sigma_0, \sigma_{45}, \sigma_{90}, \sigma_b, R_0, R_{45}, R_{90}$) are provided, the material constants in Hill's quadratic yield function/flow potential Φ_{2Y}, Φ_{2P} and Gotoh's quartic yield function Φ_4 with reduced anisotropy are readily computed from simple algebraic relations [37]. For parameter identification on AA6111-T4 sheet in this study, the yield stress under equal biaxial tension σ_b will be replaced by the shear yield stress under pure shear $\sigma_{s0} = 105.1$ MPa estimated approximately from simple shear experiments using DD2A and DD1B samples. As the uniaxial tensile yield stresses and plastic strain ratios of AA6111-T4 sheet used in this study are $(\sigma_0, \sigma_{45}, \sigma_{90}) = (174.1, 173.4, 166.7)$ MPa and (R_0, R_{45}, R_{90})=(0.93,0.41,0.66), the material constants for Hill's yield function/flow potential and Gotoh's yield function from these seven experimental inputs are subsequently obtained as

$$\begin{aligned} &Y_1 = 1, \quad Y_2 = -1.0513, \quad Y_3 = 1.0908, \quad Y_4 = 2.9929, \\ &P_1 = 1, \quad P_2 = -0.9637, \quad P_3 = 1.2120, \quad P_4 = 2.2718, \end{aligned} \tag{18}$$

$$\begin{aligned} &A_1 = 1, \quad A_2 = -1.9275, \quad A_3 = 2.7102, \quad A_4 = -1.8921, \quad A_5 = 1.1897, \\ &A_6 = 5.8027, \quad A_7 = -2.5785, \quad A_8 = 6.1468, \quad A_9 = 5.8085. \end{aligned} \tag{19}$$

The positivity and convexity of these calibrated yield functions are readily established (see [34, 36, 37]). If the AA6111-T4 sheet material is subjected to an on-axis pure shear in stress ($\sigma_1 = -\sigma_2$, $\theta = 0^o$), then the ratio of corresponding principal plastic strains $\dot{\varepsilon}_2/\dot{\varepsilon}_1$ via Eqs. $(11)_1$ and $(13)_1$ in Section Principal Plastic Strain Increment Ratio in Pure Shear Stressing would be -1.059, -1.143 and -1.040 as predicted by the calibrated Hill's yield function Φ_{2Y}, Hill's flow potential Φ_{2P} and Gotoh's yield function Φ_4. On the other hand, if the AA6111-T4 sheet material is subjected

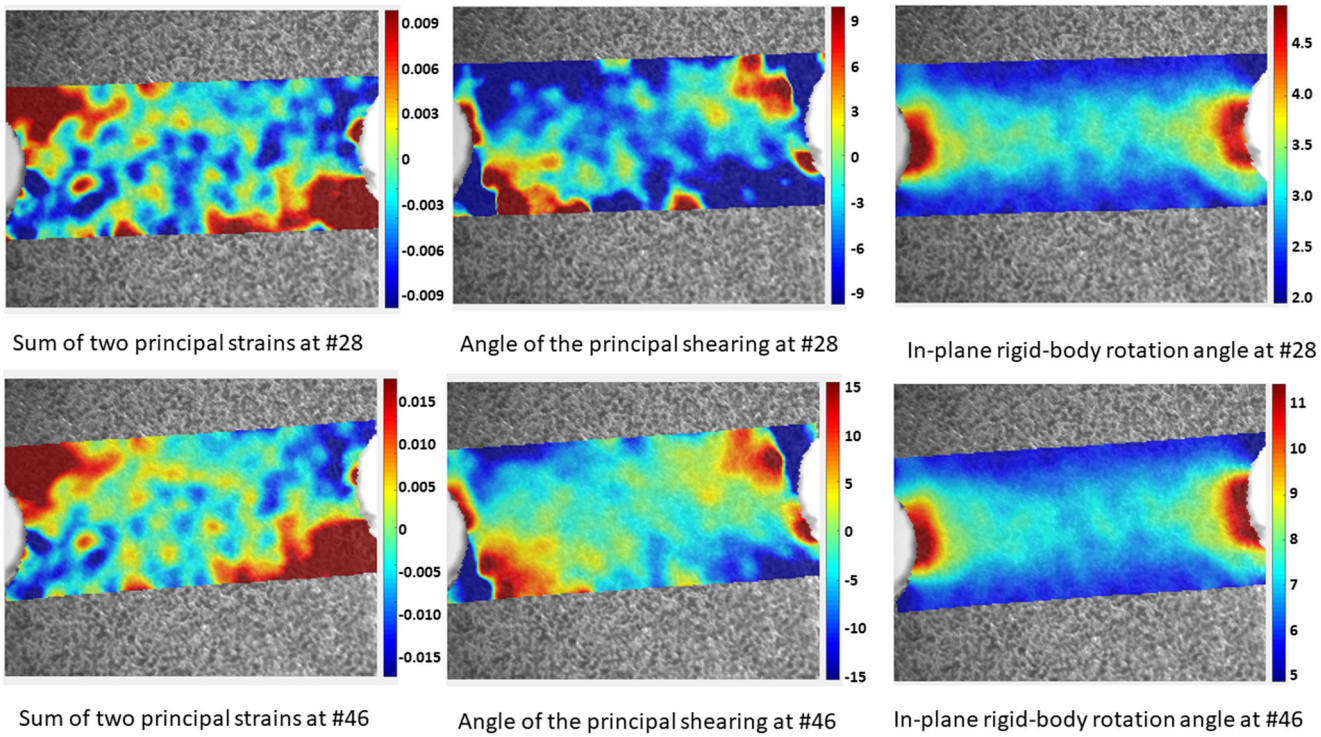

Fig. 13 Three additional maps from the whole-field strain measurements for DD2A sample from image frame No.28 and No.46: **a** the sum of two in-plane principal strains (left); **b** the angle in degree of the principal shearing plane deviating from the horizontal direction (middle); **c** the angle in degree of the in-plane rigid-body rotation due to shearing (right)

to an on-axis pure shear straining ($\dot{\varepsilon}_1 = -\dot{\varepsilon}_2,\ \theta' = 0^o$), then the ratio of corresponding principal Cauchy stresses σ_2/σ_1 via Eq. $(15)_1$ and Eq. $(17)_1$ in Section Principal Stress Ratio in Pure Shear Straining would be -0.84, -0.71 and -0.914 as predicted by the calibrated Hill's yield function Φ_{2Y}, Hill's flow potential Φ_{2P} and Gotoh's yield function Φ_4. The shearing test experiments described in the previous section were carried out under a fixed tensile loading direction and would be more closely approximated as a pure shear in stress especially at the initial stage of the shearing tests. The full-field strain mapping measurements of two shear samples DD2A and DD1B as presented in the previous section show that the resulting deformation in their shearing zones are close to but nevertheless clearly different from $\dot{\varepsilon}_2/\dot{\varepsilon}_1 = -1$ or $\dot{\varepsilon}_1 + \dot{\varepsilon}_2 = 0$, more consistent with the model predictions here assuming approximately on-axis pure shear in stress (neglecting the elastic strains as usual).

Implications of the newly proposed shear constraint

As shown by the results of both Hill's quadratic and Gotoh's quartic models in Section Modeling Pure Shear by Hill's Quadratic and Gotoh's Quartic Anisotropic Plastic Models, pure shear stressing and straining are found to be indeed identical when the shearing direction is parallel either to the rolling or to the transverse direction of a sheet metal (i.e., the loading angle $\theta = \pm 45^o$). This is in fact true for any orthotropic plasticity model when the applied Cauchy stress $\boldsymbol{\sigma} = (\sigma_x, \sigma_y, \tau_{xy}) = (0, 0, \pm\tau)$ or the applied plastic strain increments $\dot{\boldsymbol{\varepsilon}} = (\dot{\varepsilon}_x, \dot{\varepsilon}_y, \dot{\varepsilon}_{xy}) = (0, 0, \pm\dot{\gamma}/2)$. However, a general pure shear stressing condition in terms of the intrinsic variables $(\sigma_1, \sigma_2) = (\tau, -\tau)$ and $\theta \neq \pm 45^o$ does not lead to a pure shear straining state, see Eqs. $(11)_1$, $(11)_3$, $(13)_1$ and $(13)_3$. Similarly, a general pure shear straining condition in terms of the intrinsic variables $(\dot{\varepsilon}_1, \dot{\varepsilon}_2) = (\dot{\gamma}/2, -\dot{\gamma}/2)$ and $\theta' \neq \pm 45^o$ does not always generate a pure shear stressing state, see Eqs. $(15)_1$, $(15)_3$, $(17)_1$ and $(17)_3$.

For the 45-degree and 135-degree pure shear stressing conditions considered in Sections Two Types of Pure Shear Loading Conditions on a Sheet Metal and Modeling Pure Shear by Hill's Quadratic and Gotoh's Quartic Anisotropic plastic models ($\theta = \theta' = 0^o$ or 90^o), one has to set following conditions on material constants (Y_1, Y_3) for the associated Hill's model, (P_1, P_3) for the non-associated Hill's model, and (A_1, A_2, A_4, A_5) for the associated Gotoh's model respectively to generate a pure shear straining state ($\dot{\varepsilon}_1^{ps} + \dot{\varepsilon}_2^{ps} = 0$) per Eqs $(11)_1$, $(11)_3$, $(13)_1$ and $(13)_3$

$$Y_1 = Y_3, \quad P_1 = P_3, \quad 2A_1 - A_2 = 2A_5 - A_4. \tag{20}$$

Similarly, for the 45-degree and 135-degree pure shear straining conditions considered in Sections Two Types of Pure Shear Loading Conditions on a Sheet Metal and Modeling Pure Shear by Hill's Quadratic and Gotoh's Quartic Anisotropic Plastic Models, one has to set the same conditions above on material constants for Hill's and Gotoh's models to generate a pure shear stressing state ($\sigma_1^{ss} + \sigma_2^{ss} = 0$) per Eqs. $(15)_1$, $(15)_3$, $(17)_1$ and $(17)_3$. This effectively reduces the total number of independent on-axis polynomial coefficients in Hill's 1948 quadratic and Gotoh's 1977 stress functions from 3 to 2 and from 5 to 4 respectively. When the proposed shear constraint was applied to the non-quadratic yield function YLD2000-2D under the pure shear loading cases #1 and #3 by Abedini et al. [2], it also reduced its total number of independent material constants from 8 to 7.

Recall that the plastic strain ratio $R_b = \dot{\varepsilon}_2/\dot{\varepsilon}_1$ under equal biaxial tension $\sigma_2 = \sigma_1$ is given by these two yield functions as [32, 33]

$$R_b = \frac{P_2 + 2P_3}{2P_1 + P_2}, \quad R_b = \frac{A_2 + 2A_3 + 3A_4 + 4A_5}{4A_1 + 3A_2 + 2A_3 + A_4}, \tag{21}$$

the imposed condition of $Eq.(20)_2$ by the new shear constraint would imply $R_b = 1$ for Hill's quadratic yield function as well. In fact, Abedini et al. [2] suggested that under pure shear stressing $\sigma_1 = -\sigma_2$, a sheet metal should undergo only pure shear straining $\dot{\varepsilon}_1 = -\dot{\varepsilon}_2$ as well and vice versa for *all loading angles* (i.e., not limited only to 0^o, 45^o and 90^o as considered above so far). By transforming Hill's quadratic flow potential function into a form in terms of intrinsic variables, one can show that the ratio of axial plastic strain increments $\dot{\varepsilon}_2/\dot{\varepsilon}_1$ is given as (under the off-axis pure shear stressing condition of $\sigma_1 = -\sigma_2$ and $0^o < \theta < 45^o$ or $45^o < \theta < 90^o$)

$$\frac{\dot{\varepsilon}_2}{\dot{\varepsilon}_1} = -\frac{P_1 - P_2 + P_3 + P_4 - 2(P_1 - P_3)\cos 2\theta + (P_1 - P_2 + P_3 - P_4)\cos 4\theta}{P_1 - P_2 + P_3 + P_4 + 2(P_1 - P_3)\cos 2\theta + (P_1 - P_2 + P_3 - P_4)\cos 4\theta}. \tag{22}$$

That is, either $2\theta = 90^o$ or the shear constraint condition of $Eq.(20)_2$ will be sufficient to make it to be -1 (pure shear straining). Here the shearing strain $\dot{\varepsilon}_{12}$ due to the off-axis loading is assumed to be negligible for simplicity. Similarly, one obtains the following condition for Gotoh's yield function if $\dot{\varepsilon}_1 + \dot{\varepsilon}_2 = 0$ when $\sigma_1 = -\sigma_2$

$$\cos 2\theta = 0, \quad \text{or} \quad 2A_1 - A_2 + A_4 - 2A_5 = 0, \quad A_6 - A_8 = 0. \tag{23}$$

So one additional condition on the two off-axis polynomial coefficients A_6 and A_8 is needed to meet the shear constraint $\dot{\varepsilon}_2/\dot{\varepsilon}_1 = -1$ for the loading angles other than 0^o, 45^o and 90^o. It is interesting to note that such a condition had indeed previously been assumed for a version of Gotoh's yield function with reduced anisotropy [20, 35].

A non-zero hydrostatic stress $\sigma_1 + \sigma_2 \neq 0$ due to in-plane pure shear straining and a non-zero thickness strain increment $\dot{\varepsilon}_1^p + \dot{\varepsilon}_2^p \neq 0$ due to in-plane pure shear stressing can exist in plane stress (with $\sigma_3 = 0$) for an orthotropic sheet metal per both Hill's quadratic and Gotoh's quartic models. That is, even when the principal stress axes $\sigma_1\sigma_2$ and principal plastic strain increment axes $\dot{\varepsilon}_1\dot{\varepsilon}_2$ in on-axis pure shear are coincided with each other (if the shearing directions are the same in both loading conditions), the induced principal plastic strain increment ratio $(\dot{\varepsilon}_2/\dot{\varepsilon}_1)_{ps}$ and the induced principal stress ratio in pure shear $(\sigma_2/\sigma_1)_{ss}$ are in general not equal to -1. They are not some non-physical artifacts as claimed by Abedini et al.[2] but are instead some unique and intrinsic features due to the anisotropic nature of a sheet metal. Per simple logic, the equivalence of pure shear stressing and straining claimed by Abedini et al.[2] for a non-quadratic *isotropic* plasticity model such as Hosford's model cannot be used to justify its validity for either quadratic or non-quadratic *anisotropic* plasticity models at all. As isotropic plasticity models are only a subset of anisotropic plasticity models, their insistence on the equivalence of pure shear stressing and straining conditions is not warranted for anisotropic sheet metals in general. In other words, the proposed shear constraint is neither a first level constraint (positivity and convexity) nor a second level constraint (pressure-independent plastic incompressibility, an associated or a non-associated plastic flow) as discussed in Introduction that one shall commonly impose on anisotropic plasticity modeling of sheet metals. It is instead a third-level provisional constraint of reduced anisotropy between no anisotropy (isotropy) and full anisotropy for a given orthotropic yield function.

Concluding remarks

When a typical set of seven experimental inputs $(\sigma_0, \sigma_{45}, \sigma_{90}, \sigma_b, R_0, R_{45}, R_{90})$ are made available, the polynomial coefficients for both Hill's 1948 quadratic and Gotoh's 1977 quartic yield functions are readily determined directly from a set of algebraic equations without the unnecessary shear constraint imposed [37]. In this study, it is shown that the shear yield stress under on-axis pure shear σ_{s0} estimated approximately from a shearing experiment using either Type A or Type B sample geometry may substitute the yield stress under equal biaxial tension σ_b in parameter identification of both yield functions. The shearing experiments on AA6111-T4 sheet presented in this study show that the actual loading conditions and deformation states of the shearing zone in sheet metal samples are rather complex. They may be approximated to a certain degree as pure shear in stress $(\sigma_2/\sigma_1 \approx -1)$ but clearly deviate from pure shear in straining (i.e., $\varepsilon_2/\varepsilon_1 \neq -1$). That is, limited by the experimental uncertainties of full-field strain measurements, one cannot unequivocally confirm that the ideal pure shear condition of $\varepsilon_2/\varepsilon_1 = -1$ has been uniformly and strictly achieved inside the gauge section of those two types of simple shear test coupons at low and moderate shear strain levels.

In conclusion, while the so-called shear constraint proposed by Abedini et al.[2] or some other similar third level constraints may be imposed for a subset of orthotropic materials or for some heuristic reasons such as when there are insufficient experimental inputs for fully calibrating an anisotropic yield function [37], such a constraint is definitely not physically necessary due to lack of supporting experimental evidence in general and is overly restrictive in the context of modeling sheet metals with seven experimental inputs using either Hill's quadratic or Gotoh's yield quartic functions.

Compliance with Ethical Standards

Conflict of interests The authors declare that they have no conflict of interest.

Appendix

The yield functions and/or flow potentials of both associated and non-associated Hill's 1948 quadratic plasticity models and the associated Gotoh's quartic plasticity model are briefly summarized here (for details with related formulas for their parameter identification, see [32, 35, 37]).

Hill's 1948 quadratic yield stress function in plane stress is given in a compact form as

$$\Phi_{2y}(\sigma_x, \sigma_y, \tau_{xy}) = Y_1\sigma_x^2 + Y_2\sigma_x\sigma_y + Y_3\sigma_y^2 + Y_4\tau_{xy}^2, \quad (24)$$

where Y_1, Y_2, Y_3 and Y_4 are its four material constants, $f(\boldsymbol{\sigma})$ (where $\Phi_{2y}(\boldsymbol{\sigma}) = f^2(\boldsymbol{\sigma})$) is the equivalent yield stress appeared in the rate-independent yield condition $f(\boldsymbol{\sigma}) - \sigma_f = 0$, and σ_f is called the yield strength of the sheet metal.

A quadratic flow potential $\Phi_{2p}(\boldsymbol{\sigma})$ is of the same polynomial form and it is given as

$$\Phi_{2p}(\sigma_x, \sigma_y, \tau_{xy}) = P_1\sigma_x^2 + P_2\sigma_x\sigma_y + P_3\sigma_y^2 + P_4\tau_{xy}^2, \quad (25)$$

where P_1, P_2, P_3 and P_4 are its four material constants. When the yield condition is met, plastic strain increments can then be computed via the flow rule $\dot{\boldsymbol{\varepsilon}}^p = \lambda\partial g/\partial\boldsymbol{\sigma}$ with $\lambda \geq 0$ as the plastic loading variable and $\Phi_{2p}(\boldsymbol{\sigma}) = g^2(\boldsymbol{\sigma})$. For the classical associated Hill's quadratic model, $\Phi_{2p} = \Phi_{2y}$. Otherwise, different Φ_{2y} and Φ_{2p} constitute the non-associated quadratic model with a total of seven independent material constants.

Gotoh's quartic yield stress function has the following form

$$\Phi_4(\sigma_x, \sigma_y, \tau_{xy}) = A_1\sigma_x^4 + A_2\sigma_x^3\sigma_y + A_3\sigma_x^2\sigma_y^2 + A_4\sigma_x\sigma_y^3 + A_5\sigma_y^4 + A_6\sigma_x^2\tau_{xy}^2 + A_7\sigma_x\sigma_y\tau_{xy}^2 + A_8\sigma_y^2\tau_{xy}^2 + A_9\tau_{xy}^4, \quad (26)$$

where A_1, A_2,... and A_9 are its nine material constants. In an associated quartic model, the above yield stress function are used to define the equivalent yield stress and flow potential of homogeneous degree one in stress that are used in the yield condition and flow rule respectively, namely, $\Phi_4(\boldsymbol{\sigma}) = f^4(\boldsymbol{\sigma}) = g^4(\boldsymbol{\sigma})$. A simpler version of Gotoh's yield function with reduced anisotropy can be fully calibrated using only a total of seven independent material constants as well [35, 37].

References

1. ASTM B831-19 (2019) Standard Test Method for Shear Testing of Thin Aluminum Alloy Products. ASTM International, West Conshohocken, PA, www.astm.org
2. Abedini A, Butcher C, Rahmaan T, Worswick M (2018) Evaluation and calibration of anisotropic yield criteria in shear loading: Constraints to eliminate numerical artefacts. Int. J. Solids and Structures 151:118–134
3. Bae DH, Ghosh AK (2003) A planar simple shear test and flow behavior in a superplastic Al-Mg alloy. Metall. Mater. Trans. 34A:2465–2471
4. Balawender T (2005) A comparison of a tensile test with a planar simple shear test in sheet metals. Scientific Bulletin Series C 19:1–6
5. Barlat F, Kim DJ (2016) Advanced constitutive modeling and application to industrial forming processes. MATEC Web of Conferences (NUMIFORM2016) 80:15013
6. Barlat F, Maeda Y, Chung K, Yanagawa M, Brem JC, Hayashida Y, Lege DJ, Matsui K, Murtha SJ, Hattori S, Becker RC, Makosey S (1997) Yield function development for aluminum alloy sheets. J. Mech. Phys. Solids 45(11/12):1727–1763
7. Blaber J, Adair B, Antoniou A (2015) Ncorr: Open-source 2D digital image correlation Matlab software. Exp Mech 55(6):1105–1122
8. Bouvier S, Haddadi H, Levee P, Teodosiu C (2006) Simple shear tests: Experimental techniques and characterization of the plastic anisotropy of rolled sheets at large strains. J. Mater. Proc. Tech. 172:96–103
9. Drucker DC (1959) A definition of stable inelastic material. ASME. J. Appl. Mech. 26:101–106
10. Gardner KA, Seidt JD, Isakov M, Gilat A (2014) Characterization of sheet metals in shear over a wide range of strain rates. Dynamic Behavior of Materials 1:313–317
11. Gotoh M (1977) A theory of plastic anisotropy based on a yield function of fourth order (plane stress state) I & II. Int. J. Mech. Sci. 19:505–520
12. Guner A, Zillmann B, Lampke T, Tekkaya AE (2014) In-situ measurement of loading stresses with X-ray diffraction for yield locus determination. Int J Automot Technol 15:303–316
13. Hibbeler R (2014) Mechanics of materials, Ninth Edition. Prentice Hall, New York
14. Hill R (1948) A theory of the yielding and plastic flow of anisotropic metals. Proc. Royal Soc, London n193:281–297
15. Hill R (1950) The mathematical theory of plasticity. Clarendon Press, Oxford
16. Hill R (1958) A general theory of uniqueness and stability in elastic-plastic solids. J. Mech. Phys. Solids 6:236–249
17. Hill R (1979) Theoretical plasticity of textured aggregates. Math. Proc. Cambridge Philo. Soc 85:179–191
18. Hill R (1987) Constitutive dual potentials in classical plasticity. J. Mech. Phys. Solids 35(1):23–33
19. Hill R (1990) Constitutive modeling of orthotropic plasticity in sheet metals. J. Mech. Phys. Solids 38:403–417
20. Hu W (2003) Characterized behaviors and corresponding yield criterion of anisotropic sheet metals. Mater Sci Eng A345:139–144
21. Hubnatter W, Merklein M (2008) Characterization of material behavior under pure shear condition. Int J Mater Form 1:233–236
22. Kang J, Wilkinson DS, Wu PD, Bruhis M, Jain M, Embury JD, Mishra RK (2008) Constitutive behavior of AA5754 sheet materials at large strains. ASME Journal of Engineering Materials and Technology 130 031004–1–031004–5
23. Lubliner J (1990) Plasticity theory. Macmillan, New York
24. Maugin GA (1992) The thermomechanics of plasticity and fracture. Cambridge University Press, Cambridge, UK
25. Miyauchi K (1984) A proposal of a planar simple shear test in sheet metals. Sci. Papers Inst. Phys. Chem. Res. 78:27–40
26. Ogden RW (1984) Non-Linear Elastic deformations. John Wiley & Sons, New York
27. Pacheco AA, Batra RC (2008) Instabilities in shear and simple shear deformations of gold crystals. J. Mech. Phys. Solids 56:3116–3143
28. Pan B, Li K, Tong W (2013) Fast, robust and accurate digital image correlation calculation without redundant computation. Exp Mech 53:1277–1289
29. Peirs J, Verleysen P, Degrieck J (2012) Novel technique for static and dynamic shear testing of Ti6Al4V sheet. Exp Mech 52:729–741
30. Rauch EF (1998) Plastic anisotropy of sheet metals determined by simple shear tests. Mater. Sci. Engng. A 241:179–183
31. Tong W (2013) Formulation of Lucas–Kanade digital image correlation algorithms for non-contact deformation measurements: a review. Strain 49:313–334
32. Tong W (2016) Application of Gotoh's orthotropic yield function for modeling advanced high-strength steel sheets. ASME Journal of Manufacturing Science and Engineering 138:094502–1
33. Tong W (2016) Generalized fourth-order Hill's 1979 yield function for modeling sheet metals in plane stress. Acta Mech 227(10):2719–2733
34. Tong W (2018) Algebraic convexity conditions for Gotoh's non-quadratic yield function. ASME Journal of Applied Mechanics 85:074501–1
35. Tong W (2018) An improved method of determining Gotoh's nine material constants for a sheet metal with only seven or less experimental inputs. International Journal of Mechanical Sciences 140:394–406
36. Tong W (2018) On the certification of positive and convex Gotoh's fourth-order yield function. J. Phys.: Conf. Ser. 1063:012093
37. Tong W, Alharbi M (2017) Comparative evaluation of non-associated quadratic and associated quartic plasticity models for orthotropic sheet metals. Int. J. Solids and Structures 128:133–148
38. Tozawa N (1978) Plastic deformation behavior under the conditions of combined stress. In: Koistinen DP, Wang NM (eds) Mechanics of sheet metal forming, pp 81-110, Plenum Press, New York
39. Vegter H, van den Boogaard AH (2006) A plane stress yield function for anisotropic sheet material by interpolation of biaxial stress states. Int J Plast 22:557–580

40. Wu H, Xu Z, Wang PT (1998) Torsion test of aluminum in the large strain range. Int. J. Plasticity 13:873–892
41. Yang G, Sheng J, Tong W, Carlson BE, Wang HP, Kovacevic R (2018) Tensile behavior of fusion-brazed aluminum alloy coach-peel joints fabricated by a dual-beam laser. Journal of Materials Processing Tech. 261:184–192
42. Yeoh OH (2001) Analysis of deformation and fracture of 'pure shear' rubber testpiece. Plastics, Rubber and Composites 30:389–397